

Turbulent flow-field effects in a hybrid CFD-CRN model for the prediction of NO_x and CO emissions in aero-engine combustors

A. Innocenti^a, A. Andreini^{a,*}, D. Bertini^a, B. Facchini^a, M. Motta^b

^a*Department of Industrial Engineering DIEF, University of Florence, Via di Santa Marta 3, 50139 Florence, Italy*

^b*GE Avio S.R.L. - Via I Maggio, 99, 10040, Rivalta di Torino (TO), Italy*

Abstract

The paper presents a numerical study where a hybrid CFD-Chemical Reactor Network (CRN) approach is used to predict pollutant emissions in a tubular combustor for aero-engine applications. A fully-automated clustering of the simulated flow field with the generation of a reactor network representative of the main flow features is exploited. Similar cells are detected and grouped using a two step approach, the first one based only on aerodynamic criteria for turbulent flows followed by a chemical refinement based on mixture fraction. A formulation for turbulent diffusion fluxes is introduced in the reactor code to model species and energy exchanges between reactors. Three different operating conditions are studied for which measured NO_x and CO are available. Results highlight the importance of including turbulent diffusion in the network solution. The accurate prediction of pollutant emissions at different load points confirms that CFD-CRN is a valid and flexible approach for preliminary assessment of aero-engine combustor emissions in the design phase.

Keywords: Chemical Reactor Network, CFD; combustor, aeroengine, Gas Turbine, emissions, spray flame, liquid fuel, PSR, PFR, NO_x

1. Introduction

One of the main targets for the next generation of civil aero-engines is the abatement of engine pollutant emissions, in particular NO_x , to meet the stringent regulations to be implemented in the near future. The most prominent way to achieve the compliance is represented by lean burn technology.

Therefore, huge efforts have been put in developing injection strategies (i.e. lean direct injection systems) that create a lean burning mixture directly inside the combustion chamber by improving the rate of spray evaporation and fuel air mixing.

An example of such a technology is the so-called PERM injector developed by GE-Avio. The PERM injector (Partially Evaporating and Rapid Mixing), investigated in this paper, is a double swirler airblast atomizer developed to achieve partial evaporation inside the inner duct and rapid mixing within the combustor, optimizing the location and stability of the flame. Further details about the PERM injector can be

*Corresponding Author

Email address: antonio.andreini@unifi.it (A. Andreini)

Nomenclature

\dot{m}	Mass Flow Rate [kg/s]	P	Pressure [bar]
ϕ	Equivalence Ratio[-]	$PERM$	Partial Evaporation and Rapid Mixing
τ	Residence Time [s]	PFR	Plug Flow Reactor
CFD	Computational Fluid Dynamics	PSR	Perfectly Stirred Reactor
CRN	Chemical Reactor Network	RTD	Residence Time Distribution
EDC	Eddy Dissipation Concept	T_3	Air Inlet Temperature [K]
EI	Emission Index [g/kg_{fuel}]	V	Volume [m^3]

12 found in [1] and [2].

13 Combustor design process requires a rapid and accurate estimate of the main performance and emission
14 indices. To this end, Computational Fluid Dynamic (CFD) and in particular Reynolds Averaged Navier
15 Stokes (RANS) approaches have been used extensively as a standard predictive tool for combustion applica-
16 tions at industrial levels. Even if RANS approaches remain a valid choice to provide fast indications [3, 4, 5],
17 the accurate prediction of pollutants emissions requires the use of detailed chemical reaction mechanisms
18 thus leading to very high computational costs.

19 Recently the use of tabulated chemistry methods such as ISAT [6] or FGM [7], allows handling detailed
20 chemistry limiting CFD computational costs. However, the usual assumption of considering the flame in the
21 thin laminar flamelet regime (high Damkholer numbers) wrinkled by turbulence does not allow to capture
22 low Damkholer number reactions, such as those involved in NO_x formation. Some formulations have been
23 proposed to fix this aspect [8], [9], but a general solution is far to be available.

24 In last years, a new family of approaches was conceived, based on the use of CFD in conjunction with
25 Chemical Reactor Networks (CRNs).

26 Several applications of equivalent reactor network to lean-premixed combustors, diffusion flames or Rich
27 Quench Lean combustors for aero-engines can be found in literature [10, 11, 12].

28 The hybrid approach was first introduced by Ehrhardt et al. [13] and it is based on three main steps: first,
29 a CFD simulation of the reactive flow field is performed using a global chemical reaction scheme. The CFD
30 results are then post-processed applying a set of global criteria to separate the combustor in chemically and
31 physically homogeneous zones. The cells that satisfy the same criteria are clustered together to form the zones
32 of the reactor network. A Perfectly Stirred Reactor (PSR) or a Plug-Flow Reactor (PFR) is associated to
33 each zone according to the local flow conditions. The links and the exchanges of the main physical quantities
34 between the reactors are established by computing the mass fluxes between adjacent zones. Lastly the CRN
35 obtained is solved with a detailed chemical reaction mechanism to obtain an accurate prediction of pollutant

36 emissions.

37 Falcitelli et al. [14] defined a general algorithm to construct the CRN based on equivalence ratio and
38 temperature. The procedure was applied to industrial furnaces [15, 16] and boilers for power generation
39 [17, 18, 19]. An optimized procedure to split the reactive flow field into homogeneous zones is presented by
40 Fichet et al. [20] which applied the procedure to a gas turbine combustor in order to model NO_x formation
41 with about 400 chemical reactors.

42 Monaghan et al. [21] employed this approach to study the pathways of formation of NO and NO_2 in a
43 methane-air diffusion flame. They identified six macro-zones with a criterion based on equivalence ratio. A
44 further refinement is realised based on temperature leading to a final network of 1114 PSRs. Recently the
45 procedure has been extended to confined swirling flames [22] and to gas turbines [23, 24, 25].

46 In their study Novosselov et al. [26] defined five main regions in the combustor: a main flame zone, a
47 pilot flame zone, the center and the dome recirculation zones and the gas burn-out region. The network is
48 then refined to obtain the final configuration of 31 chemical reactor elements representing the different flow
49 and reaction zones of the combustor.

50 The advantage of having few elements in the network (some tens) is that it is possible to maintain a
51 physical interpretation of each reactor: looking at the distribution of the main quantities in the network, i.e.
52 NO_x formation rate, it is easier to obtain design indications to reduce emissions. On the other hand, in a
53 network with a limited number of elements a significant error can be introduced if the reactors are linked
54 only by the computed convective mass fluxes between adjacent zones from CFD. In this case, as it will be
55 shown in this paper, the contribution of turbulent diffusion cannot be neglected and its physical and robust
56 implementation is mandatory to provide correct results.

57 Finally, it is worth mentioning available commercial solutions for CFD-CRN procedure such as ANSYS
58 Fluent reactor network solver [27]. Clustering procedure is not based on aerodynamics and does not aim at
59 maintaining a physical meaning of each identified zone. It is based on temperature and mixture fraction and
60 a limited number of additional custom-field variables can be exploited to improve the clustering (e.g. spatial
61 coordinates or turbulent kinetic energy). Convective flows through reactors are computed from CFD using
62 a standard approach while diffusion fluxes are neglected. Only PSR reactors are employed. Energy equation
63 is not solved and the temperature in each reactor can be either fixed at a constant value derived by CFD or
64 calculated from the equation of state, retrieving pressure from the CFD solution.

65 The aim of the present work is the study of pollutant emissions of an aero-engine combustor at different
66 operating conditions, representative of real flight operations, exploiting an integrated CFD-CRN modelling
67 approach. A fully automated routine for the CFD postprocess and the network generation is developed for
68 a tubular combustor with a swirling jet undergoing vortex breakdown, though it can be easily adapted to
69 annular combustors. The splitting criteria are based on flow and mixing quantities only. Variables such
70 as temperature or species concentrations that are directly influenced by the CFD simplified mechanism are
71 avoided. The target is the generation of a CRN with few reactors to keep the physical interpretation of each

72 branch of the network. The network is then solved in an in-house code, REACT, developed by Andreini and
 73 Facchini [12] and further improved in Andreini et al. [28]. In the present work, the original code has been
 74 upgraded with the inclusion of turbulent diffusion. The implementation is then validated and emphasis is
 75 put on its crucial role for the correct prediction of species and heat fluxes in the reactor network.

76 Direct comparisons of the results with available measured emissions at the combustor outlet shows en-
 77 couraging results.

78 The paper is organized as follows: the investigated geometry is presented in Section 2. The methodology
 79 is then introduced starting from a description of the CFD setup (Section 3.1), the CFD post processing
 80 and network generation (Section 3.2) and the mathematical model of the reactor network as well as the
 81 implementation of turbulent diffusion in the REACT code (Section 3.3). Finally, in Section 4 the main
 82 assessment and results are presented before reporting the main conclusions.

83 2. Investigated combustor

84 The methodology is applied to study a lean spray flame generated by GE-Avio advanced PERM injection
 85 system in a laboratory test case.

86 The PERM injector, schematically represented in Figure 1 together with the investigated test-rig, is a
 87 double radial co-rotating swirler where liquid fuel is mainly injected by a prefilming airblast scheme. A
 88 film of fuel is generated over the inner surface of the lip that separates the two swirled flows. As the film
 89 reaches the edge of the lip primary atomization occurs: fine droplets and rapid mixing are promoted by the
 90 two co-rotating swirled flows generated by the double swirler configuration. To ensure a stable operation of
 91 the lean burn system the airblast injector is coupled with a hollow cone pressure atomizer (pilot injector)
 92 located at centre of primary swirler, which generates a pilot flame to stabilize the combustion process in a
 93 configuration usually referred to as "piloted airblast".

94 The PERM combustor rig was installed and tested at ONERA Palaiseau Center (see Figure 1). The
 95 combustor consists in a cylindrical flame tube with a length to diameter ratio L/D equal to 3.25. Air enters
 96 the combustion chamber through the swirled channels of the injector and through a slot located in the corner
 97 between the dome and the liner, which discharges the air flow used for the impingement cooling of the dome.

98 Standard measurement of emissions (CO , NO_x , UHC) at the combustor outlet were obtained at ONERA
 99 during NEWAC EU project and made available for this work by GE-Avio (for more details on the rig refer
 100 to [29]).

101 Three different operating conditions, respectively representative of Idle (Point 1), Cruise (Point 2) and
 102 Take-off (Point 3), have been investigated. The main operating parameters for the three cases are summarized
 103 in Tab. 1 where also the measured NO_x and CO are reported in terms of Emission Index (EI_X), defined as
 104 follows:

$$EI_X = 1000 \frac{\dot{m}_X}{\dot{m}_{fuel}} \left[\frac{g}{kg} \right] \quad (1)$$

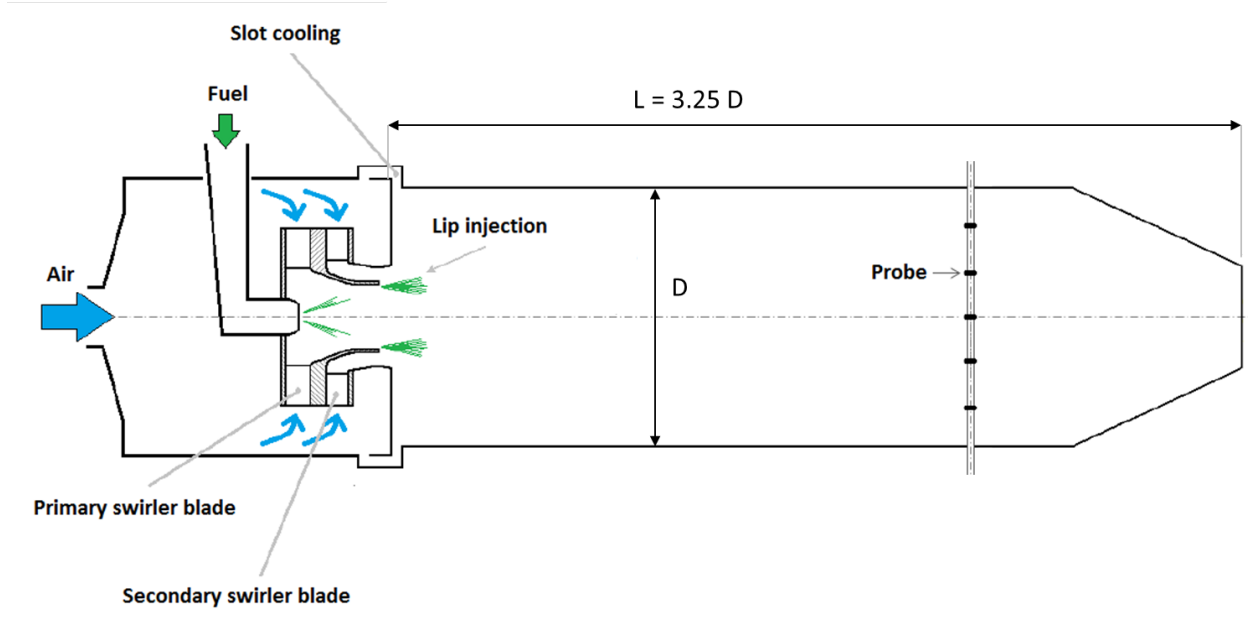


Figure 1: Sketch of the studied tubular combustor equipped with a single PERM injector.

Test Point	$P[\text{bar}]$	ϕ	$T_3[\text{K}]$	$Pilot[\%]$	EI_{CO}	EI_{NO}
Point 1	5.3	0.599	613	20	14.23	3.59
Point 2	13.5	0.570	656	15	2.12	10.87
Point 3	22.4	0.520	811	15	0.91	26.16

Table 1: Operating parameters for the tested operating conditions. T_3 is the inlet air temperature, ϕ is the overall combustor outlet equivalence ratio and $Pilot$ is the pilot to total fuel mass flow rate percentage.

105 3. CFD-CRN Procedure

106 A schematic representation of the CFD-CRN workflow is illustrated in Figure 2.

107 The procedure consists of three main steps. A CFD simulation of the combustor is performed at first. As
 108 a second step, the CFD solution is postprocessed to generate the chemical reactor network. In this phase,
 109 the computational cells are clustered into homogeneous regions associated to specific reactors of the network.
 110 Reactors properties and their flow connections are also computed in the post-process operation and used to
 111 define the network topology. Finally, the generated network is solved in a dedicated code, called REACT,
 112 with a detailed mechanism.

113 A detailed description of the three steps is given in the following sections.

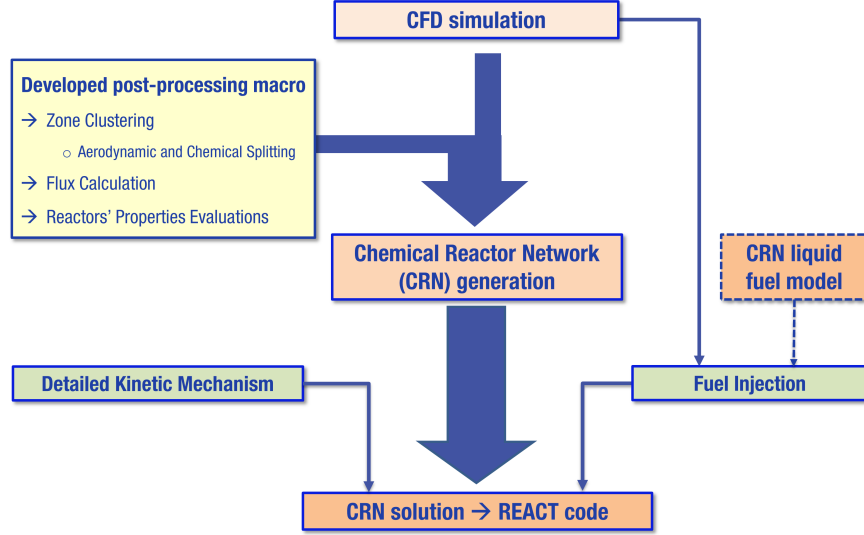


Figure 2: Flow diagram of the coupled CFD-CRN procedure.

114 3.1. CFD simulations: numerical models

115 In the present study, RANS solutions are obtained using the commercial solver ANSYS CFX v16.2 [30].
 116 Time-averaged Navier-Stokes equation are solved together with the additional scalar RTD, Residence Time
 117 Distribution, which represents the flow age since the instant of injection, and a set of passive scalars (tracers):
 118 a distinct tracer is injected from each air inlet to track the corresponding air stream. A coupled solver is
 119 used for pressure-velocity coupling and a second order accurate finite volume method is employed for all the
 120 equations.

121 Only a sector slice domain of 1.5° is simulated to reduce computational costs. The computational mesh
 122 counts about 60000 hexahedral cells with a single element in the azimuthal direction. The mesh was realized
 123 in order to have nearly isotropic volumes in the region where the flame is developing (up to $L/D = 1.5$). A
 124 sensitivity study on the mesh element size was carried out looking also at the effect on spray evolution. An
 125 hexahedral element of 0.4 mm was considered for the final setup which is below the size where appreciable
 126 differences can be observed: some details about the mesh sensitivity on a similar case are reported in [31]
 127 and [32].

128 A specified mass flow rate is assigned on all the air inlets. A simplified representation of the swirler vanes
 129 is realized, as depicted in Figure 3. Swirler air is injected by two distinct inlets located at the exit section
 130 of each vane row. The flow split between primary and secondary swirlers and flow directions is retrieved by
 131 preliminary simulations of the full 360° combustor, including the upstream plenum (see [2] for details). A
 132 third air inlet is included for the slot cooling. A constant static pressure is imposed at the domain outlet.
 133 At the lateral surfaces periodic boundary conditions are assigned while walls are considered adiabatic.

134 Concerning the employed models, the $k - \omega$ SST turbulence model [33] with a wall-function approach
 135 is used together with the Eddy Dissipation Concept (EDC) combustion model [34]. A transport equation

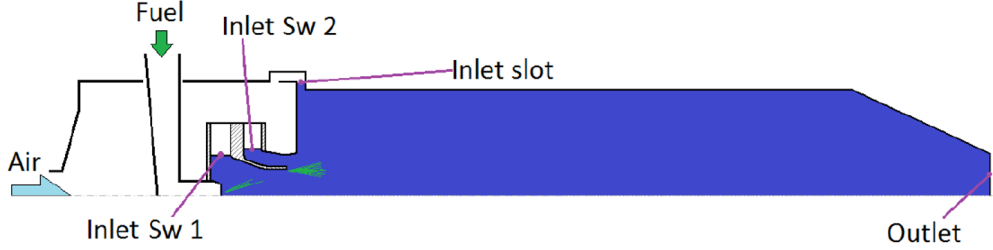
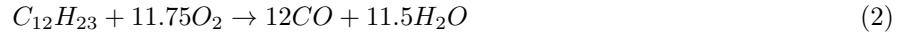


Figure 3: Sketch of the considered computational domain.

136 is solved for each species present in the used skeletal reaction scheme and therefore complex mechanisms
 137 are prohibitive for the high computational cost and numerical stiffness introduced. Finite rate kinetics is
 138 considered by computing the source term as the minimum between a turbulent mixing term and a standard
 139 Arrhenius one.

140 JetA-1 fuel is modelled by a single species surrogate: $C_{12}H_{23}$ whose transport properties for both liquid
 141 and vapor phases are computed accordingly to Rachner [35]. A two-step global mechanism for $C_{12}H_{23}$ is
 142 employed, which consists in a first step for fuel oxidation into CO and H_2O , and a second step for CO
 143 oxidation into CO_2 :



144 Arrhenius coefficients for this scheme can be found in [36].

145 A two-way Eulerian-Lagrangian particle tracking approach is considered for the solution of spray dynamics
 146 and two-phase flow physics. Pressure atomizer injection is realized injecting a statistically representative
 147 population of parcels using a hollow cone model with a 45° cone angle. The main injection is modelled with a
 148 surface injection at the lip tip where the primary breakup occurs. Particles are introduced with a 0° injection
 149 angle and a temperature of 298 K. For the droplet size distribution, a Rosin Rammler probability density
 150 function is used with a mean droplet size of $92.55 \mu m$ and a spread parameter of 2. Secondary breakup
 151 effects are considered through the well-known Taylor Analogy Breakup (TAB) model [37]. The dispersion of
 152 particles due to turbulence in the fluid phase is included using the Random Walk model [38].

153 3.2. CFD post processing and network generation

154 CFD solutions provide information about flow field and chemistry, which are used to perform the zone
 155 splitting, build a CRN and compute reactors properties. The CFD post processing is based on a two-step
 156 approach: a first aerodynamic splitting and a further refinement based on mixture fraction.

157 1. Aerodynamic splitting

158 In this phase a first combustion zoning is performed by looking at typical aerodynamic quantities
 159 such as velocity, turbulence kinetic energy, turbulence length scales, RTD and tracers. The main

160 regions associated to the combustor aerodynamics are then identified: principal inlet streams, high
 161 speed swirling jet, inner and corner recirculation regions, burnout region. In Figure 4 the obtained
 162 aerodynamic clustering is shown.

163 The criteria used to clustering cells, which are briefly presented in the following, are specified through
 164 User Defined Limits (UDL) to apply at flow variables (e.g. UDL_{T1} is a User Defined Limit for *Tracer1*
 165 concentration, UDL_{AV} is a User Defined Limit for the axial velocity, and so on). Acting on the UDLs
 166 it is possible to adapt the subdivision to the investigated case, maintaining the same aerodynamic
 167 structures.

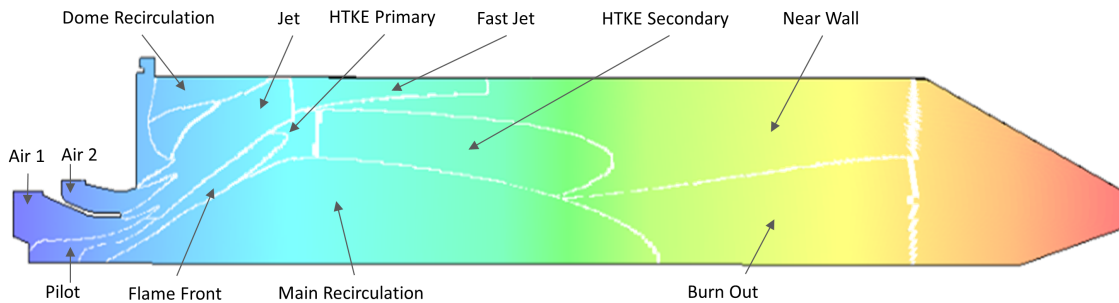


Figure 4: Aerodynamic splitting obtained for the studied combustor equipped with a PERM injector.

- 168 • *Air inlets* regions are identified by high concentration of tracking scalars (e.g., $Air\ 1 \rightarrow Tracer1 < UDL_{T1}$).
- 169
- 170 • *Jet and Peripheral Jet*: they constitute the main flame zone and are identified by the highest
 171 velocity in the domain (e.g., $Jet \rightarrow AxialVelocity > UDL_{AV}$).
- 172 • *Main and Dome Recirculation* are identified by negative axial velocity and high flow age
 173 ($AxialVelocity < 0$ and $RTD > UDL_{RDT}$).
- 174 • *Flame Front and High Turbulence Kinetic Energy (HTKE) Regions* are characterised by the high-
 175 est levels of turbulence kinetic energy, due to the shears between the vortex breakdown and the
 176 swirled jet (e.g., $Flame\ Front \rightarrow TKE > UDL_{TKE}$). Intense reaction rates are found in here.
 177 The reacting mixture feeds the inner recirculation and sustains the main flame.
- 178 • *Near Wall, Burn Out and Final* constitute the post-flame and burn out regions. Among the
 179 remaining cells, they are distinguished by a different flow age. The *Near Wall* region, in fact, is
 180 mainly fed by the "young" fast jet bypassing the inner recirculation.

181 2. Chemical splitting

182 The main features of the vortex breakdown stabilised flame are identified by this first clustering. A
 183 further refinement is realized in this second phase based on mixture fraction, according to what proposed
 184 by Monaghan et al. [21]. In this step homogeneous cells from a chemical kinetic point of view are
 185 grouped.

186 Once the cell clustering is completed a reactor is associated to each region. Reactor properties (residence
187 time, volume etc.) and exchanged mass flows are computed. Based on this, connections are established
188 between reactors.

189 Looking at Figure 5 two different problems are now analyzed. Firstly, to correctly reproduce the flow
190 exchanges among recirculation regions, three zones are defined: the recirculation zone with negative axial
191 velocity (PSR-2), one zone that collects the mass flow coming from the former (PSR-1a) and a third one that
192 delivers back mass flow to the recirculation region (PSR-1b).

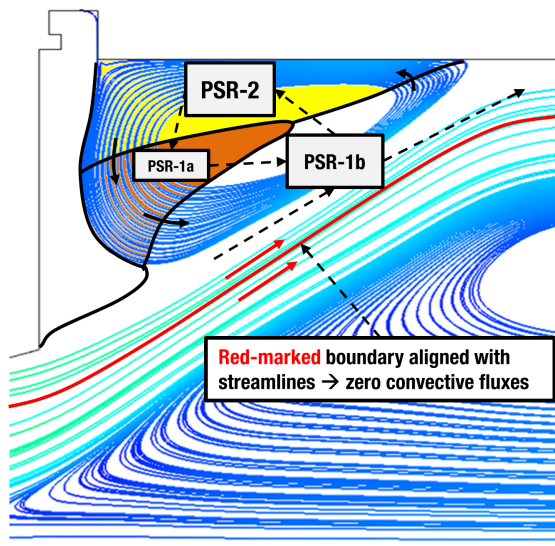


Figure 5: Example of region splitting to account for flow recirculation. Red line highlights a region boundary aligned with streamlines.

193 Secondly, if the interface of two adjacent regions is aligned with the flow streamlines we run into the
194 limit situation where the computed mass flow will be zero. In this situation species and energy exchanges
195 are mainly governed by turbulent diffusion. Establishing connections in the CRN based on convective mass
196 flows alone this contribution is missed and the fluxes are not correctly represented. This is a key observation
197 that points out the importance of including such a contribution in the CRN solution and that gives reason
198 to the development introduced in REACT code (see section 3.4).

199 3.3. The reactor network model

200 Once the cell clustering is completed a chemical reactor is associated to each region. The in-house code
201 REACT is used to solve the network. The code is based on CHEMKIN II libraries ([39]) and handles
202 both PSR and PFR models, which are both implemented with two different concepts. The first concept
203 considers standard ideal micro-mixing which does not allow to take into account liquid fuel injection, while a
204 second approach, proposed by Prior et al. [40], allows to model liquid fuel evaporation and non-ideal mixing
205 associated to it. Further details about numerical tool can be found in Andreini et al. [28]. In the present work

206 only ideal PSR and PFR reactors are used and the liquid fuel injection is not modelled inside the network.

207 The reactor network is created employing PSR in all the identified regions except for the burn-out ones
 208 close to the outlet (post-flame) where PFRs are used to complete the combustion. The choice of PSRs is
 209 particularly justified in the primary zone of the combustor, which typically includes large recirculation regions
 210 and requires sufficient residence time and high turbulence levels.

211 Appropriate residence times for each reactor are selected based on CFD computed flowfield. Following the
 212 approach proposed by Fichet et al. [20], a transport equation is solved in the CFD simulation for a passive
 213 scalar, RTD [s], which represents the mean age of the flow. A source term is introduced in RTD transport
 214 equation that increases its value of 1 each second, thus representing the linear dependence of the fluid age
 215 on time.

216 In each region the mean residence time (ΔRTD) is computed as the average of the pass-through times
 217 of the streamlines on the region itself:

$$\Delta RTD = \frac{\oint \dot{m} RTD}{\frac{\oint \dot{m}}{2}} \quad (4)$$

218 The solved equations for PSRs are the conservation of the k -th species and energy:

$$\frac{dY_k}{dt} = \frac{dY_k}{\tau} - \frac{dY^{(in)_k}}{\tau} + \frac{\dot{\omega}_k W_k}{\rho} + S_k^{diff} \quad (5)$$

$$\frac{dT}{dt} = \frac{1}{\tau c_p} \sum_{k=1}^K \left[Y^{(in)_k} \left(h^{(in)_k} - h_k \right) \right] - \frac{1}{\tau c_p} \sum_{k=1}^K W_k h_k \dot{\omega}_k + Q_Y^{diff} + Q_T^{diff} \quad (6)$$

219 where Y_k is the mass fraction the k -th species, $Y^{(in)_k}$ the inlet mass fraction, τ the reactor residence time,
 220 ρ the average density of the reactor mixture, $\dot{\omega}_k$ the chemical source term of the k -th species with molecular
 221 weight W_k , T is the temperature, c_p the average specific heat at constant pressure for the reactor mixture
 222 and h_k is the enthalpy. S_k^{diff} in Eq. 5 and Q_Y^{diff} and Q_T^{diff} in Eq. 6 are related to turbulent diffusion. For
 223 their expressions please refer to the dedicated section 3.4.

224 In a PFR, purely convective one-dimensional flow is assumed. Species and energy equations are solved
 225 along with the mass and momentum conservation in the following form:

$$u \frac{\partial Y_k}{\partial x} = \frac{\dot{\omega}_k W_k}{\rho} \quad (7)$$

$$\bar{c}_p \frac{\partial T}{\partial x} + u \frac{\partial u}{\partial x} + \sum_{k=1}^K h_k \frac{\partial Y_k}{\partial x} = 0 \quad (8)$$

226 where x is the direction of the flow and u is the axial velocity.

227 For the two type of reactors, temperature is the main quantity driving chemical reactions and its wrong
 228 prediction can lead to inaccurate pollutant evaluations, especially for NO_x emissions. In REACT code, the
 229 reactor temperature can be either fixed at the value obtained by reference CFD calculation or computed by

230 solving energy conservation inside the code. In contrast to most literature approaches, in the present work
 231 the energy conservation is solved in the network. In this way the predicted temperature and its effects on
 232 intermediate and dissociation reactions on the temperature are taken into account to obtain more accurate
 233 values for both temperature and species concentrations.

234 A chemical reaction mechanism based on a single element surrogate for Jet-A fuel, i.e. $C_{12}H_{23}$, involving
 235 16 species and 39 reactions is used in the present work [41]. It includes both the thermal [42] and prompt
 236 [43] pathways for NO_x formation. Similar results have been obtained testing other mechanisms, i.e. Leeds
 237 scheme for $C_{10}H_{22}$ (see [44]) and the reaction set reported in [45] for the same surrogate species. Results
 238 are not reported here as the sensitivity to different surrogate species and different mechanisms is out of the
 239 scope of the present research.

240 The continuity, species and energy conservation equations for each reactor, which is assumed to be adia-
 241 batic, are solved in REACT. The solution for the first reactor of the network is subsequently passed to the
 242 adjacent reactors and the reciprocal interaction between them is established by the exchanged mass flow.
 243 This iterative process is considered converged when the maximum residual among temperature and species
 244 is less than 10^{-6} .

245 3.4. Diffusion fluxes modelling in chemical reactors network

246 The implementation of turbulent diffusion in the CRN solving procedure is a key development of the
 247 present research. The inclusion of diffusion fluxes in the CFD-CRN coupling is crucial to correctly model
 248 the interactions between adjacent regions, as observed in the part dedicated to the cell clustering (see section
 249 3.2).

250 In some applications (e.g. [21]) the turbulent diffusive mass flow between two reactors is calculated
 251 through the indirect use of a Peclet number (Pe) as follows:

$$\dot{m}^{diff} = \frac{\dot{m}^{adv}}{Pe} \quad (9)$$

252 where \dot{m}^{adv} is the computed convective mass flow.

253 With a null convective mass flow, i.e. when the interface between two regions in the CFD is aligned with
 254 the flow streamlines (see Figure 5), such an approach would return a zero diffusion flux. Therefore, a more
 255 physics-based formulation of turbulent diffusion is introduced in REACT code for PSRs reactors.

256 In the typical equations for PSRs (eqs. 5 and 6) the source terms S_k^{diff} , Q_Y^{diff} and Q_T^{diff} are introduced,
 257 where $S_k^{diff} = \frac{\dot{m}_k^{diff}}{\rho}$ represents the mass balance for species k due to turbulent diffusion. Generally, in
 258 a CFD RANS context based on eddy viscosity turbulence models, this contribution can be related to the
 259 gradient of the mean value of species mass fraction:

$$\dot{m}_k^{diff} = AD_T \frac{\partial Y_k}{\partial x_i} = A \frac{\mu_T}{Sc_T} \frac{\partial Y_k}{\partial x_i} \quad (10)$$

260 where A is the area of exchange, D_T the diffusion coefficient, defined as the ratio of the turbulent viscosity
 261 μ_T and the turbulent Schmidt number Sc_T .

262 When implemented in REACT code, the mass flux of the k species is computed as follows:

$$\dot{m}_k^{diff} = \sum_j^{N_{reactors}} = A_{ij} \frac{\mu_T}{Sc_T} \frac{Y_{j,k} - Y_{i,k}}{Dist_{ij}}. \quad (11)$$

263 $\frac{Y_{j,k} - Y_{i,k}}{Dist_{ij}}$ is the difference between the mass fractions of the i -th and the j -th reactors while $Dist_{ij}$ is a
 264 characteristic length.

265 Solving for the i -th reactor, the diffusion fluxes with all the other $N_{reactors}$ reactors are evaluated. The
 266 contact area A_{ij} and μ_T are computed from the CFD, at each interface. The Sc_T number is assumed constant
 267 (typically in the range of 0.7-0.9) or it can be computed from the CFD as well. If i -th and j -th reactors
 268 are not connected, the computed area A_{ij} will be zero and so the diffusion flux. The sum of the diffusion
 269 fluxes of all the k species is null ($\sum \dot{m}_{diff,k} = 0$). Therefore, including turbulent diffusion, the species are
 270 redistributed within the domain but the global mass balance of the reactor will not change.

271 The energy equation for PSR is also modified to account for heat diffusion which is computed with the
 272 following general expression:

$$q_i = \rho \sum_{k=1}^K h_k Y_k V_{k,i} - \lambda \frac{\partial T}{\partial x_i} \quad (12)$$

273 where $V_{k,i}$ is a characteristic diffusion velocity and λ the thermal conductivity. Accordingly, two contri-
 274 butions are included in eq. 6:

- 275 • Q^{diff} taking into account the flux of enthalpy due to species diffusion;
- 276 • Q^T taking into account the heat diffusion related to temperature gradients.

277 In the REACT code implementation they are expressed as follows:

$$Q_i^{diff} = \sum_{k=1}^K \sum_{j=1}^{N_{reactors}} m_{k,i,j}^{diff} [\max(0, \text{sign}(m_{k,i,j}^{diff})) C_{p_j} T_j - \min(0, \text{sign}(m_{k,i,j}^{diff})) C_{p_i} T_i] \quad (13)$$

278 and

$$Q_i^T = \sum_{j=1}^{N_{reactors}} A_{i,j} \frac{\mu_T}{Sc_T} \frac{T_j - T_i}{Dist_{ij}} \quad (14)$$

279 As for the species diffusion, the area A_{ij} and the average μ_T are computed automatically during the CFD
 280 post process routine while the Sc_T number is assumed constant and equal to 0.8.

281 **4. Results**

282 In this section the results obtained when applying the CFD-REACT procedure to study the combustor
 283 equipped with a PERM injector, are presented.

284 Firstly, the CFD results for the three tested conditions are shown and the main features of the PERM
 285 flame are described. Successively, the assessment of the implementation of diffusion fluxes in REACT is
 286 presented and finally the results obtained solving the CRNs for the test points are discussed.

287 *4.1. CFD Results*

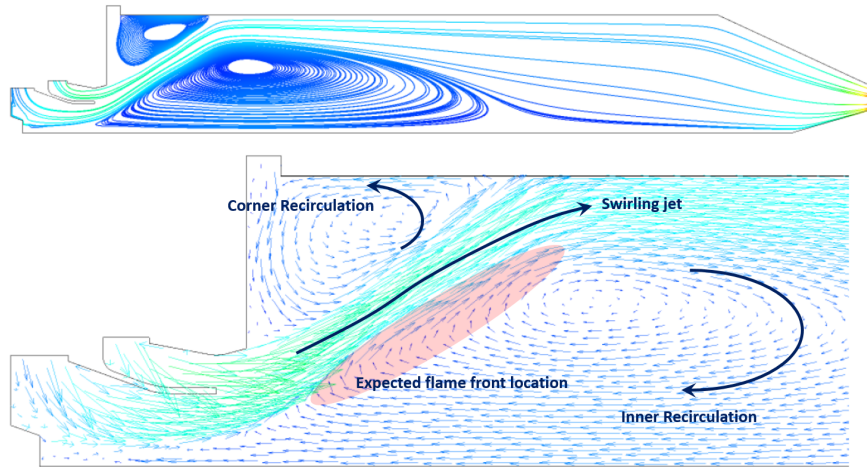


Figure 6: Main flow structures generated by PERM injector

288 The flow-field generated by the PERM injector is shown in Figure 6. The typical flow structures of swirl
 289 stabilized burners are observed. The breakdown of main swirling jet originates a large inner recirculation
 290 region and a smaller one in the external corner. The flame is expected to be stabilized by hot gases in the
 291 shear layer between the jet and the inner recirculation. These exhaust gases deliver a continuous source of
 292 ignition.

293 Temperature and mixture fraction distributions obtained for the three test points are shown in Figure 7.
 294 Temperature is normalized as follows:

$$T_{norm} = \frac{T - T_3}{T_{max} - T_3} \quad (15)$$

295 where T_{max} is the maximum flame temperature observed in the three conditions.

296 The flame shape and anchoring are highly influenced by the evaporation of droplets and vapor fuel mixing
 297 but the general structure of the flame confirms what expected by the analysis of the flowfield: a lifted partially
 298 premixed is observed, with the main flame front located in the low-velocity high-turbulence region at main
 299 recirculation zone edge. Increasing the pressure (from test Point 1 to test Point 3), the evaporation rate is
 300 enhanced and particles partially evaporate within the injector and in the first part of the jet, as shown in
 301 Figure 8. Increased particle mass sources are observed closer to the injection point. Consistently, an earlier

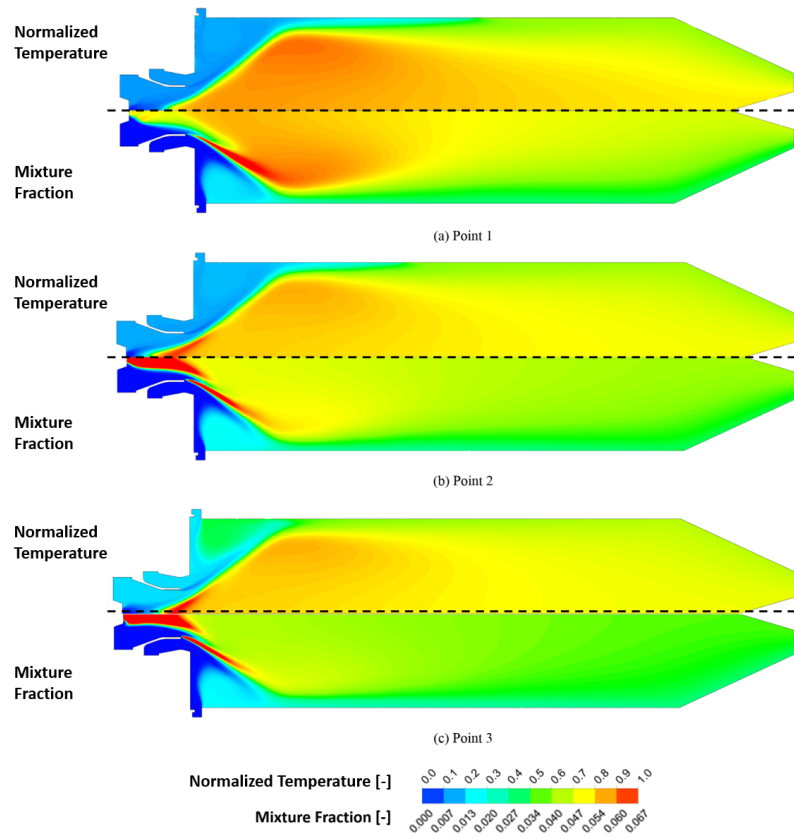


Figure 7: Normalized temperature and mixture fraction contours obtained for the simulated test points.

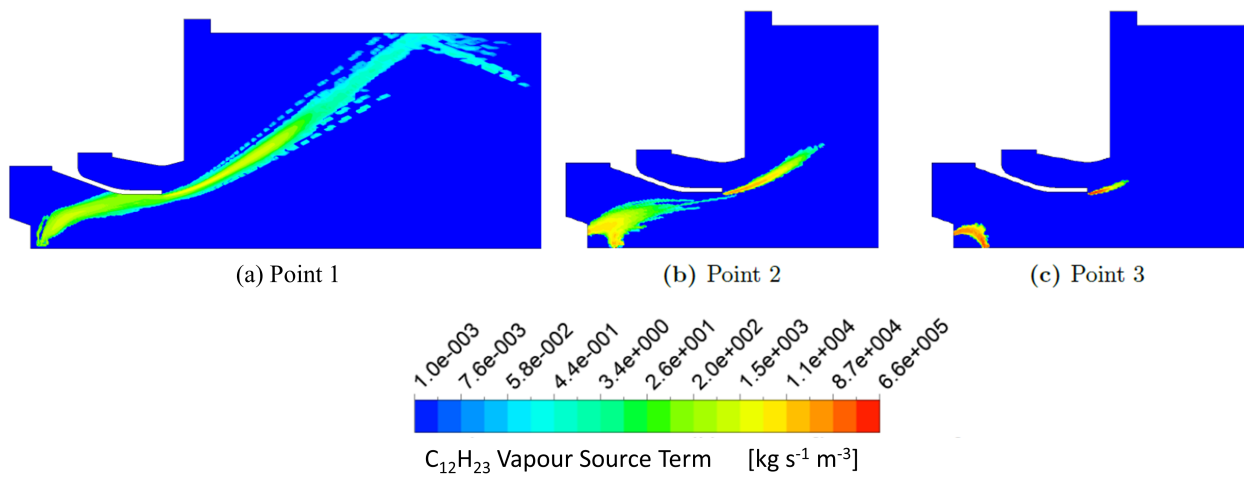


Figure 8: Predicted evaporation for the three test points at different pressure.

302 evaporation leads to a more uniform mixture fraction distribution and smoother temperatures which can be
 303 seen in Figure 7.

304 4.2. Assessment of the network generation and diffusion fluxes

305 Before presenting the final results for the three operating conditions, a general assessment of the two
 306 step clustering process and a comparison between results obtained before and after introducing the diffusion
 307 fluxes in the solution are reported here for the high pressure case (Point 3).

308 In Figure 9 the contour plots named "CFD" superimpose the clustered volume to the CFD field. Contour
 309 plots "Mean Value CFD" is obtained averaging (weighting with mass) the CFD computed distributions over
 each region.

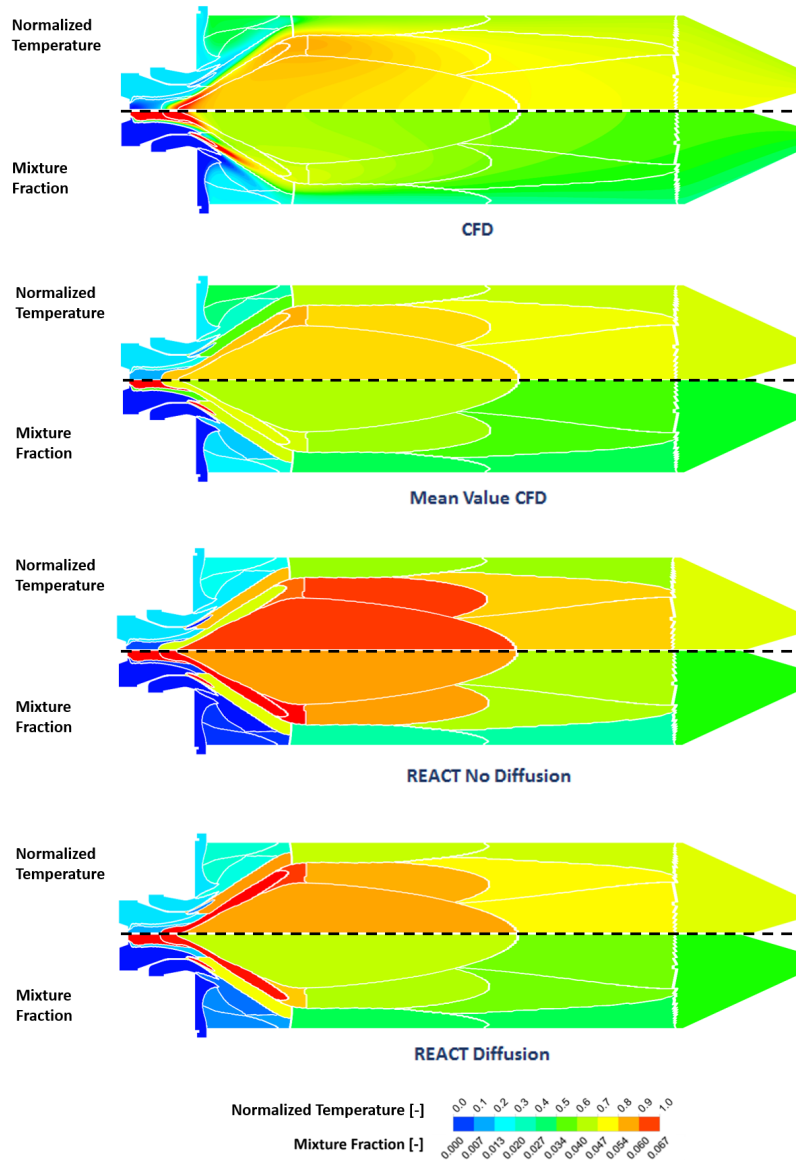


Figure 9: Comparison of temperature and mixture fraction distributions between CFD, zone-averaged CFD values and REACT results with and without diffusion.

311 Comparing the two plots, it is possible to state if the adopted refinement is representative, before freezing
312 the network and solve for it in REACT. The air-fuel mixing and the temperature levels are well reproduced
313 by the adopted clustering. In mixture fraction contours, the rich regions of pilot and main injections are
314 detected as well as the mixing with the main air along the jet. Mixture fraction and temperature levels of
315 the corner recirculation are correctly reproduced while a colder inner recirculation is predicted. Despite this
316 slight discrepancy, the accuracy obtained with the proposed clustering is retained sufficient to proceed with
317 the CRN solution.

318 Results without accounting for turbulent diffusion are shown in Figure 9 ("REACT No Diffusion" in
319 the picture). Clearly both mixing and temperatures in the network are not fully representative. The fuel
320 is injected mainly in pilot and lip regions, where fuel evaporation is predicted by CFD. Therefore, the
321 corresponding reactors are rich. However, the fuel-air mixing along the jet is not correctly modelled. As
322 the jet outer surface is aligned with the streamlines, the computed convective mass flow is small and the
323 fuel cannot go towards the corner recirculation. It is instead transported along the jet towards the inner
324 recirculation, which becomes rich. Consequently, temperature distribution in Figure 9 shows hot inner
325 recirculation and secondary HTKE regions. Temperature stratification along the radius in the final part
326 of the combustor is also missed and a uniform distribution is predicted eventually altering post flame NO_x
327 formation.

328 Introducing the turbulent diffusion fluxes, the distributions in Figure 9 ("REACT Diffusion") are ob-
329 tained. The higher the difference of species concentration between two adjacent reactors, the more intense
330 the diffusion is. Therefore, the fuel mainly flows from the rich part of the jet to the corner recirculation,
331 which is then enriched. Fuel is also taken out of the main recirculation and secondary HTKE that gets
332 leaner. Mixture fraction distribution in the network is clearly improved. This could be further adjusted
333 acting either on turbulent Schmidt number or on the characteristic distances between reactors. Both can be
334 used as network tuning parameters. Such a tuning is reasonable if the number of reactors is limited so that a
335 physical understanding is kept while adjusting the fluxes. A colder main recirculation is seen in temperature
336 distribution in Figure 9 while temperature of the corner region is slightly increased. The fuel preheating due
337 to temperature gradients is observed for pilot and main injection. The double effect of preheating the fuel
338 and of a mixture fraction closer to the stoichiometric one leads to high temperatures in the flame front. In the
339 CFD this is observed at the root of the flame. This suggests possible improvements for future development
340 of the zoning criteria such as splitting the flame front into more sub-zones. Temperature stratification in the
341 burn-out region is now captured by the network.

342 Despite a jet region with higher temperature levels and a colder dome recirculation, both mixture fraction
343 and temperature distributions in the network can be considered a good representation of the initial CFD
344 fields. The same network generation strategy is then applied to study the remaining test Points 1 and 2 at
345 lower operating pressure and to compute pollutant emissions.

346 *4.3. Comparison between the investigated test points*

347 In this section, the comparison between measured and predicted NO_x and CO, when accounting for
diffusion fluxes, is presented for the three investigated test points.

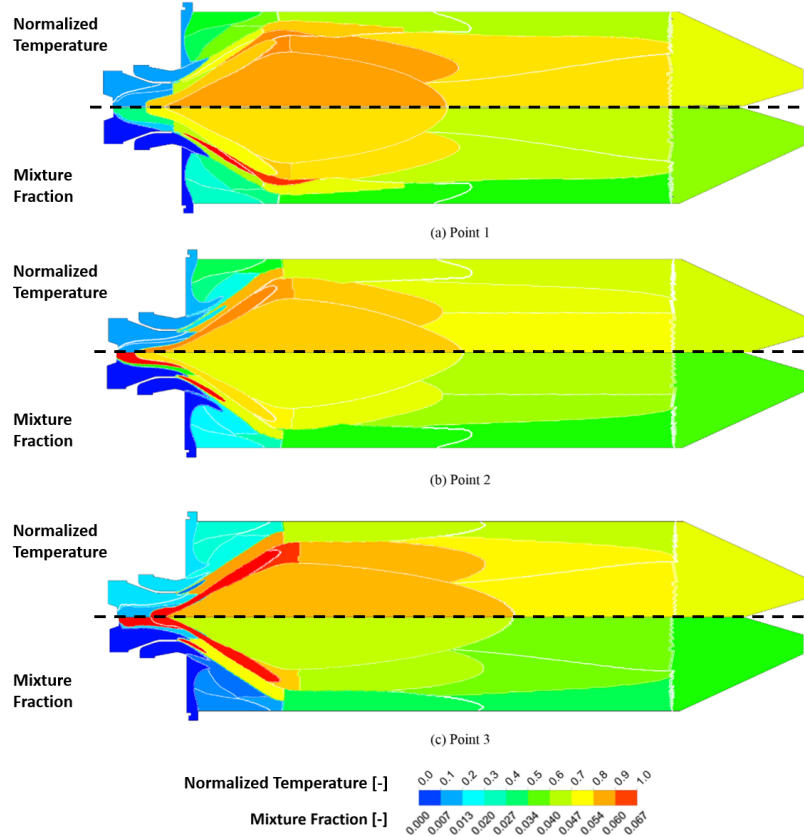


Figure 10: Temperature and mixture fraction distributions obtained in REACT for the investigated test points.

348

349 Mixture fraction and temperature distributions are shown in Figure 10 and can be directly compared to
350 CFD results reported in Figure 7. The effect of pressure on the mixing process is captured by the CFD-CRN
351 approach. The enrichment of pilot and lip injection regions with pressure is well represented in the network.
352 The rich jet observed for Point 1, due to later evaporation of the fuel droplets, as well as the enrichment
353 of the inner recirculation are reproduced. Thanks to the implemented turbulent diffusion fluxes, fuel is also
354 present in the corner region.

355 The temperature increase in the inner recirculation and inner post-flame region at low pressure is captured.
356 The intensification of the root of the flame is also reproduced even if such effect is spread over a larger region,
357 the flame front.

358 From the same picture it can be seen that a critical region to be represented is the corner recirculation.
359 The fuel is injected in the network following the evaporation pattern from CFD (see Figure 8). At low

360 pressure, the fuel vapor is carried to the corner recirculation by both convective and diffusion fluxes. On
 361 the contrary, at high pressure the fuel evaporates close to the injector and follows a way that does not allow
 362 its convective transport to such a region. Using the same tuning for the diffusion fluxes results in a richer
 363 corner zone at low pressure and a leaner zone at high pressure. A case-dependent tuning could improve the
 364 predictions.

365 In Figure 11 measured and predicted values of CO and NO_x at outlet are shown in terms of Emission Index.
 366 The predicted trend for NO_x varying the pressure is well captured and a good matching of experimental data
 367 is obtained at all the test points.

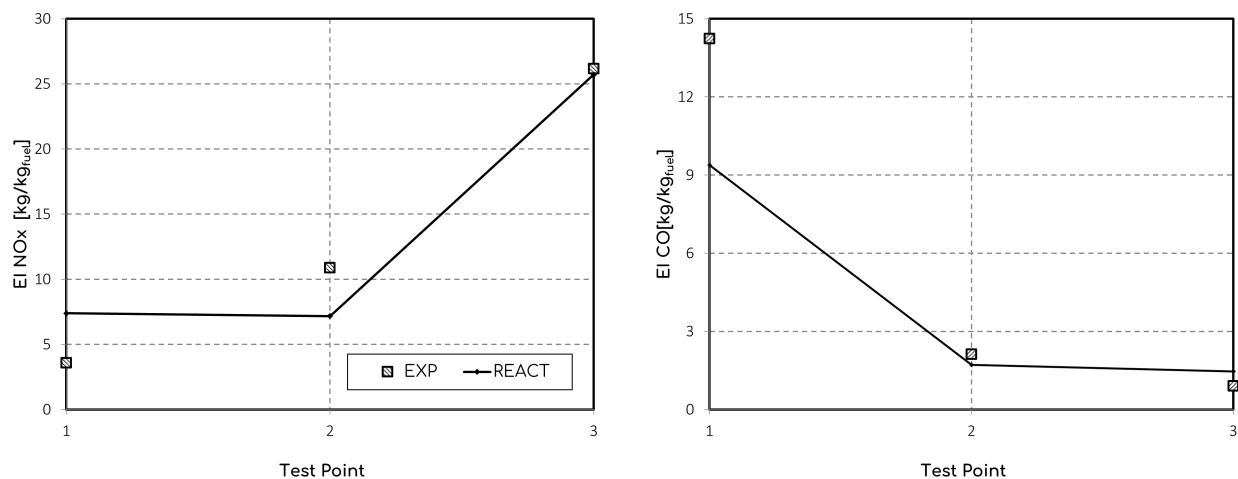


Figure 11: Measured and predicted NO_x and CO emissions for the investigated test points.

368 In Figure 12 the distribution of the source term of NO_x is shown for the investigated cases. Consistently
 369 with the temperature profiles in Figure 10, the formation of NO_x is strongly related to hot regions in the
 370 flame for all three cases. In the investigated flame, in fact, NO_x are mainly produced via thermal pathway,
 371 through the Zeldovich mechanism, which is driven by temperature levels. At low pressure, NO_x are mainly
 372 produced in the inner recirculation and post flame regions. Increasing pressure, at Point 2 and Point 3 the
 373 region of high production is moved to the flame front region and the inner recirculation. As seen in Figure
 374 10, an ongoing reaction is predicted in the corner recirculation, which is different to what predicted by CFD
 375 (see Figure 7). Nevertheless, low temperatures do not lead to NO_x production, as observed in Figure 12.

376 In general, long residence times in hot regions are critical for NO_x formation. NO maps in Figure
 377 12 suggest that a reduced NO_x production could be achieved if part of the fuel is by-passing the inner
 378 recirculation, flowing along the fast jet directly to post-flame zone. This could be obtained modifying the
 379 PERM injection design such as the injected liquid droplet are no longer trapped in the main recirculation.
 380 The present study indeed provided indications for some of the main modifications introduced in the most
 381 recent designs of PERM injector.

382 Concerning CO emissions at the outlet, reported in Figure 11, a good agreement is obtained for Point 2

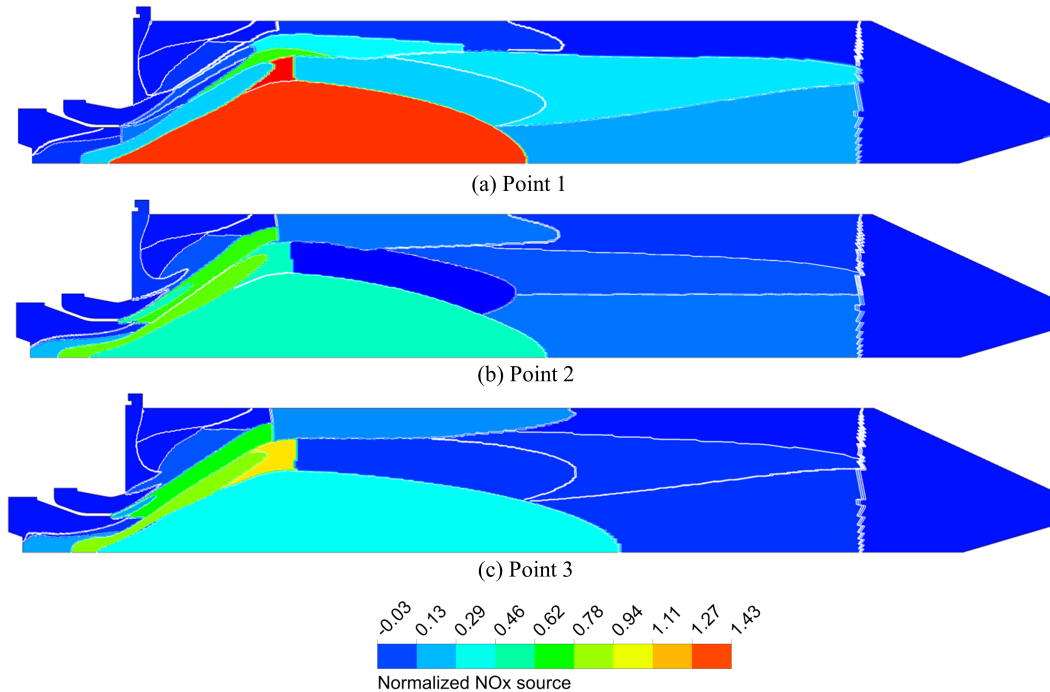


Figure 12: NO source term distributions obtained in REACT for the investigated test points.

383 and Point 3. CO at the outlet tends to reach values close to chemical equilibrium and therefore, when pressure
 384 is reduced CO increases. At the same time, lower flame temperatures induce local quenching of the reaction
 385 in the primary zone, which leads to higher CO production. The trend is well represented by the network
 386 model. However, the predicted increase is lower than in experiments. Deviations from the measured values
 387 can be ascribed to the wall thermal treatment in the model, where combustor walls are assumed adiabatic.
 388 This implies the prediction of higher temperatures and the partial messing of quenching effects. This is more
 389 evident for Point 1 where measured exhaust CO is above equilibrium values.

390 5. Conclusions

391 In the present work, a hybrid CFD-CRN approach is used to study pollutant emissions (NO_x and CO)
 392 of an aero-engine combustor at different pressures. Numerical simulations of an experimental combustor,
 393 equipped with a single GE-Avio PERM injector, are carried out for three different operating points, repre-
 394 sentative of Idle, Cruise and Take-off conditions. CFD solutions provide information for the reactor network
 395 construction. Aerodynamic-based clustering criteria are defined to realise a first macro-clustering of the CFD
 396 domain. Successively, to make the final network more representative from a chemical point of view, further
 397 refinements on mixture fraction are introduced. The final networks count a limited number of reactors that
 398 allow maintaining a physical interpretation of each of them. To model in a correct way the species and
 399 energy fluxes in the reactor network, turbulent diffusion fluxes are implemented in the existing REACT code,

400 used to solve the network with a detailed chemical reaction mechanism. Results confirms that the used
401 splitting criteria are general and can be applied at different pressure levels. The necessity to properly model
402 turbulent diffusion is highlighted as well as the great improvement introduced accounting for it. An accurate
403 prediction of the concentrations of NO_x and CO is obtained at all the pressure levels, though CO deviates
404 from experiments at low loads, due to cooling effects at the combustor walls that are not included in the
405 model. Species and temperature are reasonably reproduced in the CRN, considering the limited number of
406 reactors employed. Further improvements could be introduced with a more refined clustering and with a
407 case-dependent calibration of diffusion fluxes. The approach has great potential as it allows for fast evalua-
408 tions of emissions in reacting system and to provide indications for improvements of combustor and injection
409 system design.

410 Acknowledgements

411 The research leading to these results has received funding from the European Union Seventh Framework
412 Program (FP7/2007-2013) under grant agreement n°265586 and was conducted within the IMPACT-AE
413 (Intelligent Design Methodologies for Low Pollutant Combustors for Aero-Engines) project. The permission
414 for the publication is gratefully acknowledged by the authors. The authors want to gratefully acknowledge
415 Dr. Fabio Turrini from GE-Avio for its fundamental contribution.

416 6. References

- 417 [1] M. Kern, S. Marinov, P. Habisreuther, N. Zarzalis, A. Peschiulli, F. Turrini, Characteristics of an ultra-
418 lean swirl combustor flow by LES and comparison to measurements, in: ASME 2011 Turbo Expo:
419 Turbine Technical Conference and Exposition, American Society of Mechanical Engineers, GT2011-
420 45300, 2011.
- 421 [2] A. Andreini, C. Bianchini, G. Cacioli, B. Facchini, A. Giusti, F. Turrini, Multi-Coupled Numerical
422 Analysis of Advanced Lean Burn Injection Systems, in: ASME Turbo Expo 2014: Turbine Technical
423 Conference and Exposition, American Society of Mechanical Engineers, GT2014-26808, 2014.
- 424 [3] A. Andreini, B. Facchini, A. Innocenti, M. Cerutti, Numerical Analysis of a Low NO_x Partially Premixed
425 Burner for Industrial Gas Turbine Applications, Energy Procedia 45 (2014) 1382–1391.
- 426 [4] A. Innocenti, A. Andreini, A. Giusti, B. Facchini, M. Cerutti, G. Ceccherini, G. Riccio, Numerical
427 Investigations of NO_x Emissions of a Partially Premixed Burner for Natural Gas Operations in Industrial
428 Gas Turbine, in: ASME Turbo Expo 2014: Turbine Technical Conference and Exposition, American
429 Society of Mechanical Engineers, GT2014-26906, 2014.
- 430 [5] A. Innocenti, A. Andreini, B. Facchini, M. Cerutti, G. Ceccherini, G. Riccio, Design Improvement Survey
431 for NO_x Emissions Reduction of a Heavy-Duty Gas Turbine Partially Premixed Fuel Nozzle Operating

- 432 With Natural Gas: Numerical Assessment, *Journal of Engineering for Gas Turbines and Power* 138 (1)
433 (2016) 011501.
- 434 [6] S. Pope, Computationally efficient implementation of combustion chemistry using in situ adaptive tab-
435 ulation, *Combustion Theory and Modelling* 1 (1) (1997) 41–63.
- 436 [7] J. van Oijen, A. Donini, R. Bastiaans, J. ten Thijsse Boonkcamp, L. de Goey, State-of-the-art in premixed
437 combustion modeling using flamelet generated manifolds, *Progress in Energy and Combustion Science*
438 57 (2016) 30 – 74.
- 439 [8] A. Boucher, N. Bertier, F. Dupoirieux, A method to extend flamelet manifolds for prediction of NO_x
440 and long time scale species with tabulated chemistry, *Int. J. of Sustainable Aviation* 1 (2) (2014) 181 –
441 202.
- 442 [9] A. Ketelheun, C. Olbricht, F. Hahn, J. Janicka, NO_x prediction in turbulent flames using LES/FGM
443 with additional transport equations, *Proceedings of the Combustion Institute* 33 (2) (2011) 2975 – 2982.
- 444 [10] N. Rizk, H. Mongia, A semianalytical emission model for diffusion flame, rich/lean, and premixed lean
445 combustors, in: *ASME 1993 International Gas Turbine and Aeroengine Congress and Exposition*, Amer-
446 ican Society of Mechanical Engineers, 93–GT–128, 1993.
- 447 [11] J. Tonouchi, T. Held, H. C. Mongia, A semi-analytical finite rate two-reactor model for gas turbine com-
448 bustors, in: *ASME 1997 International Gas Turbine and Aeroengine Congress and Exhibition*, American
449 Society of Mechanical Engineers, 97–GT–126, 1997.
- 450 [12] A. Andreini, B. Facchini, Gas turbines design and off-design performance analysis with emissions evalu-
451 ation, *Journal of Engineering for Gas Turbines and Power* 126 (1) (2004) 83–91, doi:10.1115/1.1619427.
- 452 [13] K. Ehrhardt, P. Toqan, P. Jansohn, J. Teare, J. Beer, G. Sybon, W. Leuckel, Modeling of NO_x reburning
453 in a pilot scale furnace using detailed reaction kinetics, *Combustion Science and Technology* 131 (1-6)
454 (1998) 131–146.
- 455 [14] M. Falcitelli, S. Pasini, N. Rossi, L. Tognotti, CFD+ reactor network analysis: an integrated methodology
456 for the modeling and optimisation of industrial systems for energy saving and pollution reduction,
457 *Applied Thermal Engineering* 22 (8) (2002) 971–979.
- 458 [15] M. Falcitelli, L. Tognotti, S. Pasini, An algorithm for extracting chemical reactor network models from
459 CFD simulation of industrial combustion systems, *Combustion Science and Technology* 174 (11-12)
460 (2002) 27–42.
- 461 [16] M. Falcitelli, S. Pasini, L. Tognotti, Modelling practical combustion systems and predicting NO_x emis-
462 sions with an integrated CFD based approach, *Computers & chemical engineering* 26 (9) (2002) 1171–
463 1183.

- 464 [17] T. Faravelli, L. Bua, A. Frassoldati, A. Antifora, L. Tognotti, E. Ranzi, A new procedure for predicting
465 NOx emissions from furnaces, *Computers & Chemical Engineering* 25 (4) (2001) 613–618.
- 466 [18] D. Benedetto, S. Pasini, M. Falcitelli, C. La Marca, L. Tognotti, NOx emission prediction from 3-D
467 complete modelling to reactor network analysis, *Combustion Science and Technology* 153 (1) (2000)
468 279–294.
- 469 [19] T. Faravelli, A. Antichi, C. Callierotti, E. Ranzi, D. Benedetto, A kinetic study of an advanced reburning
470 process, *Combustion Theory and Modelling* 1 (4) (1997) 377–393.
- 471 [20] V. Fichet, M. Kanniche, P. Plion, O. Gicquel, A reactor network model for predicting NOx emissions in
472 gas turbines, *Fuel* 89 (9) (2010) 2202–2210.
- 473 [21] R. F. Monaghan, R. Tahir, A. Cuoci, G. Bourque, M. Furi, R. L. Gordon, T. Faravelli, A. Frassoldati,
474 H. J. Curran, Detailed multi-dimensional study of pollutant formation in a methane diffusion flame,
475 *Energy & Fuels* 26 (3) (2012) 1598–1611.
- 476 [22] A. Frassoldati, S. Frigerio, E. Colombo, F. Inzoli, T. Faravelli, Determination of NOx emissions from
477 strong swirling confined flames with an integrated CFD-based procedure, *Chemical Engineering Science*
478 60 (11) (2005) 2851–2869.
- 479 [23] I. V. Novosselov, P. C. Malte, Development and application of an eight-step global mechanism for CFD
480 and CRN simulations of lean-premixed combustors, *Journal of Engineering for Gas Turbines and Power*
481 130 (2) (2008) 021502.
- 482 [24] K. B. Fackler, M. F. Karalus, I. V. Novosselov, J. C. Kramlich, P. C. Malte, Experimental and numerical
483 study of NOx formation from the lean premixed combustion of CH4 mixed with CO2 and N2, *Journal*
484 *of Engineering for Gas Turbines and Power* 133 (12) (2011) 121502.
- 485 [25] C. Russo, G. Mori, V. V. Anisimov, J. Parente, Micro gas turbine combustor emissions evaluation using
486 the chemical reactor modelling approach, in: *ASME Turbo Expo 2007: Power for Land, Sea, and Air*,
487 American Society of Mechanical Engineers, GT2007–27687, 2007.
- 488 [26] I. Novosselov, P. Malte, S. Yuan, R. Srinivasan, J. Lee, Chemical reactor network application to emissions
489 prediction for industrial gas turbine, in: *ASME Turbo Expo 2006: Power for land, sea, and air*,
490 American Society of Mechanical Engineers, GT2006–90282, 2006.
- 491 [27] ANSYS Fluent Theory Guide version 18.0, Ansys Inc. USA .
- 492 [28] A. Andreini, A. Ceccherini, B. Facchini, F. Turrini, I. Vitale, Assessment of a set of numerical tools for
493 the design of aero-engines combustors: Study of a tubular test rig, in: *ASME 2009 Turbo Expo: Turbine*
494 *Technical Conference and Exposition*, American Society of Mechanical Engineers, GT2009–59539, 2009.

- 495 [29] A. Peschiulli, First PERM concept, Tech. Rep., Deliverable 6.2.2, NEWAC Project FP6-030876, doi:
496 <http://www.newac.eu>, 2010.
- 497 [30] ANSYS CFX-Solver Modeling Guide Release 15.0, Ansys Inc., Canonsburg, PA .
- 498 [31] A. Andreini, C. Bianchini, G. Cacioli, B. Facchini, A. Giusti, F. Turrini, Multi-coupled numerical
499 analysis of advanced lean burn injection systems, Proceedings of the ASME Turbo Expo (GT2014-
500 26808).
- 501 [32] A. Innocenti, A. Andreini, B. Facchini, A. Peschiulli, Numerical analysis of the dynamic flame response
502 of a spray flame for aero-engine applications, International Journal of Spray and Combustion Dynamics
503 9 (4) (2017) 310–329, doi:10.1177/1756827717703577.
- 504 [33] F. R. Menter, Two-equation eddy-viscosity turbulence models for engineering applications, AIAA journal
505 32 (8) (1994) 1598–1605.
- 506 [34] B. F. Magnussen, B. Hjertager, On the structure of turbulence and a generalized eddy dissipation concept
507 for chemical reaction in turbulent flow, in: 19th AIAA Aerospace Meeting, St. Louis, USA, 1981.
- 508 [35] M. Rachner, Die Stoffeigenschaften von Kerosin Jet A-1, Tech. Rep., DLR, Institut für Antriebstechnik,
509 1998.
- 510 [36] T. G. Valachovic, Numerical predictions of idle power emissions from gas turbine combustors, in: ASME
511 1993 International Gas Turbine and Aeroengine Congress and Exposition, American Society of Mechan-
512 ical Engineers, 93–GT–175, 1993.
- 513 [37] G. Taylor, The shape and acceleration of a drop in a high speed air stream, The scientific papers of GI
514 Taylor 3 (1963) 457–464.
- 515 [38] A. Gosman, E. Loannides, Aspects of computer simulation of liquid-fueled combustors, Journal of Energy
516 7 (6) (1983) 482–490.
- 517 [39] R. J. Kee, F. M. Rupley, J. A. Miller, Chemkin-II: A FORTRAN chemical kinetics package for the anal-
518 ysis of gas-phase chemical kinetics, Tech. Rep. SAND89-8009, Sandia National Laboratories, Livermore,
519 CA, USA, 1989.
- 520 [40] D. Prior, J. Swithenbank, P. Felton, The Stirred Reactor Modelling of a Low Pollution Liquid Fuelled
521 Combustor, in: AIAA 15th Aerospace Sciences Conference. Aeronautics and Astronautics, vol. 54, 1977.
- 522 [41] K. Kundu, P. Penko, S. Yang, Simplified Jet-A/air combustion mechanisms for calculation of NO (x)
523 emissions, in: 34th AIAA/ASME/SAE/ASEE Joint Propulsion Conference and Exhibit, 3986, 1998.
- 524 [42] R. K. Hanson, S. Salimian, Survey of rate constants in the N/H/O system, in: Combustion chemistry,
525 Springer, 361–421, 1984.

- 526 [43] C. Fenimore, Formation of nitric oxide in premixed hydrocarbon flames, in: Symposium (International)
527 on Combustion, vol. 13, Elsevier, 373–380, 1971.
- 528 [44] A. Kyne, M. Pourkashanian, W. C.W., Modelling soot formation in aviation fuel oxidation, in: ASME
529 Turbo Expo 2006: Power for land, sea, and air, American Society of Mechanical Engineers, GT2006–
530 90571, 2006.
- 531 [45] H. Wang, E. Dames, B. Sirjean, D. Sheen, R. Tangko, A. Violi, J. Lai, F. Egolfopoulos, D. Davidson,
532 R. Hanson, et al., A high-temperature chemical kinetic model of n-alkane (up to n-dodecane), cyclo-
533 hexane, and methyl-, ethyl-, n-propyl and n-butyl-cyclohexane oxidation at high temperatures, JetSurF
534 version 2 (2010) 19, doi:(<http://melchior.usc.edu/JetSurF/JetSurF1.1>).